Irregular and fractal resonators with Neumann boundary conditions: Density of states and localization

S. Russ,* B. Sapoval, and O. Haeberlé
Laboratoire de Physique de la Matière Condensée, CNRS Ecole Polytechnique,† 91128 Palaiseau Cédex, France
(Received 28 May 1996; revised manuscript received 15 October 1996)

Vibrations of two-dimensional systems with free irregular or fractal boundaries are studied on specific examples. The eigenmodes are calculated numerically using an analogy between Helmholtz and diffusion equations. We discuss the influence of the fractal boundary on the low-frequency part of the spectrum and on wave forms. The density of states is increased by the irregularity and exhibits oscillations at special frequencies which depend on the geometry. Surprisingly, many states are found to be confined at the fractal boundary. Increasing the perimeter fractality induces increased confinement. [S1063-651X(97)04402-4]

PACS number(s): 61.43.Hv, 43.20.+g, 63.20.Pw, 63.50.+x

INTRODUCTION

How do the properties of vibrational excitations relate to the geometry of resonators? The answer to this question is important from both the fundamental and practical points of view because systems with strongly irregular geometries are ubiquitous in nature. The emergence of fractal language permits one to discuss this question in a well-defined and documented geometrical framework [1]. Not only does fractal geometry permit a description of strong statistical irregularity but it also allows one to consider deterministic fractals as simple models for extreme geometrical disorder. If the physical properties of the objects that we consider are due to the hierarchical character of their geometry, then their physical properties can be studied on deterministic fractal objects [2]. This is, for example, the case for self-similar electrodes where the study of deterministic systems is readily applicable to random self-similar structures [3].

The idea of studying the density of states (DOS) in fractal resonators is due to Berry [4]. He formulated early conjectures about the density of states in the asymptotic (high-frequency) limit. Since then these conjectures have been modified [5]. Mathematical aspects of these questions can be found in Refs. [6–8].

Two types of resonators can be considered: mass fractals and surface fractals. Their vibrations are, respectively, named ''fractons'' [9–11] and ''fractinos'' [12,13]. In the latter reference one can find an experimental and numerical study of the vibrations of a fractal drum. In such a drum, the vibrating membrane is supported by a fractal perimeter and the amplitude of the vibration is kept equal to 0 on the contour. The modes which are solutions of the Helmholtz equation with the Dirichlet boundary condition $\Psi=0$ are called ''Dirichlet'' fractinos. These Dirichlet fractinos are also solutions of the Schrödinger equation in a two-dimensional quantum well with the same geometry. Their study can be used to understand the properties of small irregular quantum dots or wires. For example, they can help to explain electro-optical properties of porous silicon [14,15].

In this paper we consider the vibrations of a two-dimensional system obeying the Neumann boundary condition

$$\partial\Psi/\partial n=0. \tag{1}$$

These modes, which we call ''Neumann'' fractinos, could represent the transverse acoustical phonons of a two-dimensional irregular crystallite. They also represent higher-order modes in acoustical waveguides with irregular or fractal cross sections and infinite wall impedance. In that case the variable Ψ corresponds to the pressure [16].

This paper presents a study of the low-frequency eigenmodes—DOS and wave forms—of the six structures shown in Fig. 1. Systems No. 0–No. 2 are a square and two prefractals of generation 1 and 2. They have a C_4 symmetry and the corresponding degeneracies. The nonsymmetric systems No. 3–5 have no degenerate states except for accidental degeneracy.

GENERAL METHOD

We first recall the numerical method used in Ref. [12]. This method is based on the correspondence between the wave equation and the diffusion equation. We wish to solve the Helmholtz equation

$$\Delta\Psi=(1/c^2)\partial^2\Psi/\partial t^2 \tag{2}$$

using condition (1) on the boundary. Here c is a wave velocity. Instead of Eq. (2) we consider the time-dependent diffusion equation on the same domain:

$$D\Delta\Psi=\partial\Psi/\partial t, \tag{3}$$

where D is a diffusion coefficient. In Eq. (3) Ψ represents a concentration of diffusing particles which may be positive or negative and condition (1) corresponds to reflecting boundaries. The general solution of Eq. (3) is a combination of real exponentials whereas that of Eq. (2) is a combination of imaginary exponentials. Both Eqs. (2) and (3) lead to the same eigenvalue problem $\Delta\Psi_n=-(\omega_n^2/c^2)\Psi_n$ or $\Delta\Psi_n=(D\tau_n)^{-1}\Psi_n$, with the correspondence

*Electronic address: sr@pmcsun1.polytechnique.fr
†Unité associée du CNRS No. 1254.

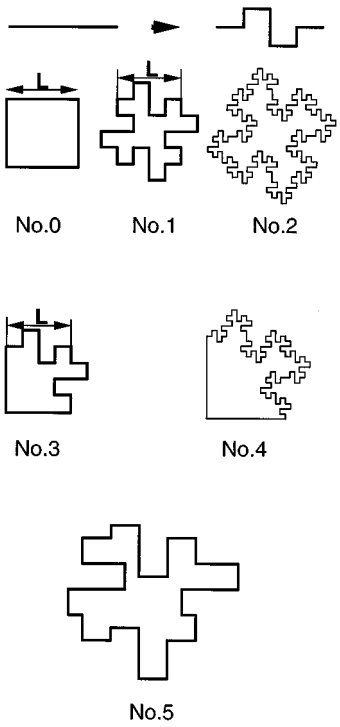

FIG. 1. Systems under study: Top: The generator for the fractal geometry and the prefractal systems No. 0, No. 1, and No. 2. The area is conserved through the iteration process. The fractal dimension of the perimeter is $D_f=\ln 8/\ln 4=3/2$. Middle: Systems No. 3 and No. 4 where the fractal generator has only been applied to two neighboring sides of the square initiator. These geometries correspond to a quarter of the systems No. 1 and No. 2. Bottom: The nonsymmetric system No. 5. It is built with segments of length 0.5, 1, and 1.5. The last three systems have no symmetry degeneracy.

$$(D\tau_n)^{-1}=\omega_n^2/c^2. \tag{4}$$

Here τ_n is the decay time constant of the diffusional eigenstate Ψ_n and ω_n is the frequency of the corresponding vibrational eigenstate.

We compute the time-dependent solution of Eq. (3), starting with an arbitrary initial function $z_0(x,y,t=0)$. The system will then converge to a function proportional to $\Psi_0(x,y)\exp(-t/\tau_0)$, yielding the first eigenstate $\Psi_0(x,y)$ with eigenvalue $1/\tau_0$ [and ω_0 through Eq. (4)] [12]. Numerically, this is verified by controlling the diffusion process until the function $z(x,y,t)$ decays everywhere exponentially with the same time constant. Then to compute the next state, we start with a new function

$$z_1(x,y,t=0)=z_0(x,y,t=0) - \Psi_0(x,y)\int \Psi_0(x,y)z_0(x,y,t=0)dx\ dy, \tag{5}$$

which is orthogonal to $\Psi_0(x,y)$. The new distribution converges to the next eigenfunction $\Psi_1(x,y)$. The procedure is then iterated by orthogonalization of the $(n+1)$th initial distribution to the n previous eigenfunctions. Numerical implementation of the above equations was made using a finite difference method and is discussed in the Appendix.

With Neumann condition a trivial eigenstate with zero frequency always exists. It represents a uniform translation of the system. This is the only state with nonzero integral, as shown by integrating the equation $\Delta\Psi_n=-(\omega_n^2/c^2)\Psi_n$ over the domain and applying the divergence theorem. We find using Eq. (1)

$$\int\int_V \Delta\Psi_n dx\ dy=-(\omega_n^2/c^2)\int\int_V \Psi_n dx\ dy = \int_\Gamma \nabla\Psi_n dl=0, \tag{6}$$

where Γ is the perimeter of the system. As ω_n^2/c^2 is nonzero for all eigenvalues, except the first one, all higher eigenmodes have zero integral over the domain.

THE LOW-FREQUENCY DENSITY OF STATES

All our resonators have the same area and to discuss the results on a single scale we use as a frequency unit the lowest eigenfrequency of the square initiator. The modes of a square with side L are labeled by the number of half wavelengths in the x,y directions $\mu,\mu'=0,1,2,\ldots$ with eigenvalues $\omega^2_{\mu,\mu'}=(\pi^2c^2/L^2)(\mu^2+\mu'^2)$. We therefore use in the following a reduced frequency $\Omega=\omega/\omega_{1,0}$ where $\omega_{1,0}=\pi c/L$ is the fundamental frequency of the square for which $\Omega^2(\mu,\mu')=(\mu^2+\mu'^2)$.

For a discretized square of side $L=Za$ (Z segments per side) the exact eigenvalues are [17]

$$\Omega_Z^2(\mu,\mu')=[2(Z+1)^2/\pi^2]\{2-\cos[\pi\mu/(Z+1)] - \cos[\pi\mu'/(Z+1)]\}. \tag{7}$$

They converge to $\Omega^2(\mu,\mu')=(\mu^2+\mu'^2)$ when Z goes to infinity. We therefore can use Eq. (7) to test the accuracy of our results as discussed in the Appendix.

We have computed the lowest eigenvalues for the systems shown in Fig. 1 (up to 100 or 200 states). The 20 lower eigenvalues for systems No. 0–2 are given in Table I in the Appendix. In our computation we have used $Z=64$ for system No. 0. The systems No. 1–4 were computed with $Z=128$. The system No. 5 was computed with the same grid density.

The numerical results for the integrated DOS of systems No. 0–2 are shown in Fig. 2. The integrated DOS $N(X)$ denotes the counting function which is the number of eigenvalues (including multiplicity) of the equation $\Delta\Psi=-X\Psi$ smaller than X. For a two-dimensional membrane, Weyl's conjecture [5,6,8] can be written, with our units

$$N(\Omega^2)=(\pi/4)\Omega^2+c(\Omega^2), \tag{8}$$

with the correction term

$$C(\Omega^2)=(L_\Gamma/4L)\Omega+(\text{higher-order terms}). \tag{9}$$

L_Γ is the length of the resonator perimeter. The relative contribution of the correction term $C(\Omega^2)$ tends to 0 when $\Omega^2\to\infty$. Note that Eq. (9) cannot be used for a mathematical fractal resonator of infinite perimeter. In this case $C(\Omega^2)$ has

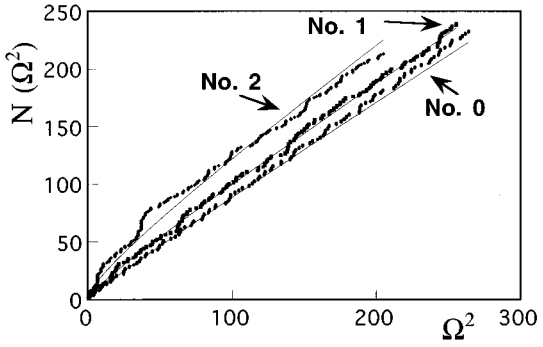

FIG. 2. Integrated DOS $N(\Omega^2)$: From bottom to top: discretized square (system No. 0), prefractal systems No. 1 and No. 2. The values calculated from the Weyl approximation [Eqs. (8) and (9)] are indicated by the continuous lines.

been proposed to be proportional to Ω^{D_f} where D_f is the Minkowski dimension of the perimeter [5,6,18]. We do not expect to really measure this effect here as our prefractal systems do not exceed the second generation [12].

Note that Eqs. (8) and (9) have been derived for continuous systems that are not exactly equivalent to our discretized systems. Furthermore, they are supposed to be valid in the asymptotic limit corresponding to small wavelengths. But this limit does not exist in discretized systems which have a cutoff frequency at $\omega_{\text{cut}}=(8k/m)^{-1/2}$. A partial theoretical analysis of the spectrum of a discrete system has been proposed by Fisher [19], but does not lead to an equivalent of Weyl's formula for discrete lattices.

In Fig. 2 we compare the computed integrated DOS $N(\Omega^2)$ of the prefractal systems No. 0–2 with the predictions of Eqs. (8) and (9). There are two main effects. First, despite the discrete character of our systems, the DOS verifies approximately Weyl's conjecture. There is a marked increase of the DOS as we pass from system No. 0 to No. 2 due to the increasing length of the frontier. This result confirms a recent observation by Hobiki, Yakubo, and Nakayama [18]: the density of states of the Neumann problem is not solely described by the first term of Eq. (8) as used in [20].

Secondly there exist steplike increases of the DOS at special frequencies. These jumps reveal the accumulation of

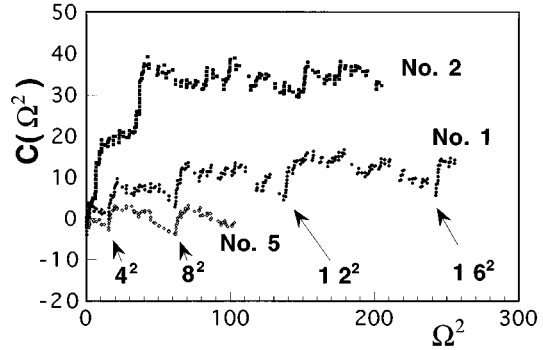

FIG. 3. Correction term $C_{\text{No.}}(\Omega^2)$ for systems No. 1, No. 2, and No. 5 obtained from Eq. (10). For systems No. 1 and No. 5 the oscillations indicated by the arrows correspond to values of $\Omega^2=L/(\lambda/2)=4, 8, 12, 16$.

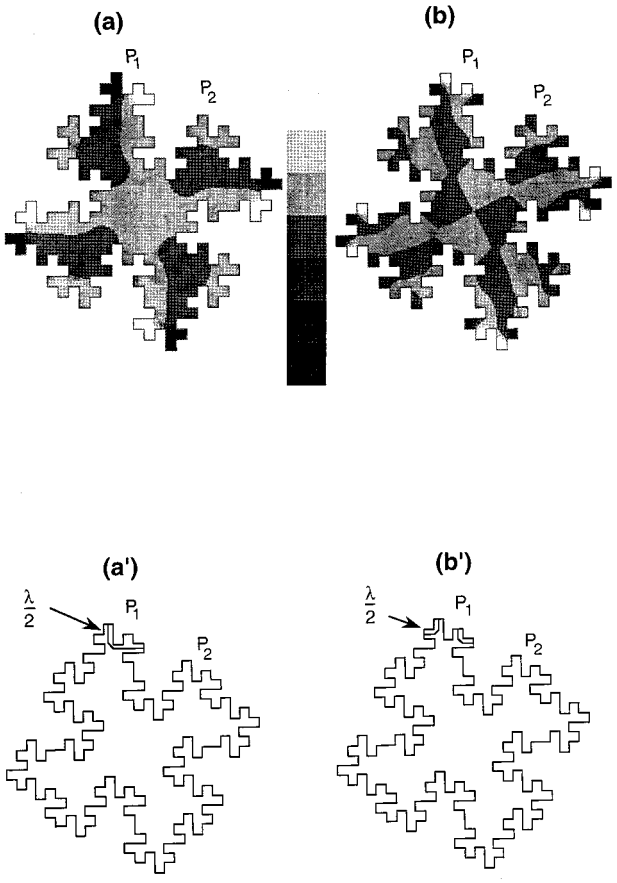

FIG. 4. Two examples of localized states—(a) state $n=17$; (b) state $n=64$. The amplitudes are indicated by different gray levels. The black and white regions stand, respectively, for positive and negative amplitudes. The gray tones stand for nearly zero amplitude. In (a′) and (b′) we show how we estimate the half wavelength $\lambda/2$ by the path length $\mathcal{L}$, leading from positive to negative amplitude regions. Regions like P_1 and P_2 may sustain quasidegenerated eigenmodes.

quasidegenerated states. To discuss more precisely the effect of the different geometries, we present in Fig. 3 the correction term $C_{\text{No. }x}(\Omega^2)$ given by

$$C_{\text{No. }x}(\Omega^2)=N(\Omega^2)_{\text{No. }x}-N(\Omega^2)_{\text{No. }0}, \tag{10}$$

where $N(\Omega^2)_{\text{No. }0}$ is the numerical DOS for the square (calculated for the same values of Ω^2 by a linear interpolation fit).

The correction term presents oscillations. For system No. 1 these oscillations correspond to values of Ω^2 that can be simply identified. Coming back to the definition of $\Omega^2=\omega^2/\omega_{1,0}^2=(2\pi c/\lambda)^2/(\pi c/L)^2=[L/(\lambda/2)]^2$ we find that these remarkable values are located at $\Omega^2=4^2$, 8^2, 12^2, 16^2. They correspond to excitations with one, two, three, or four half wavelengths in the smallest pores of width $L/4$. This behavior apparently recalls that of stable orbits in quantum chaos [21]. In this frame there should exist an accumulation of states of wavelengths corresponding to simple stable orbits of the classical system. In system No. 1, the observed accumulation of states is apparently due to the existence of eight identical pores of width $L/4$. This causes the quasidegeneracy that we observe. For each oscillation, the

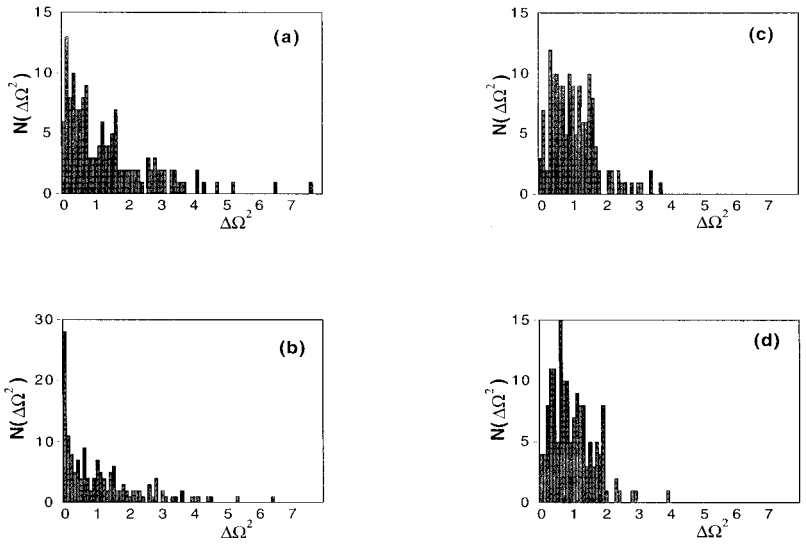

FIG. 5. Histograms of the level spacing $(\Delta\Omega^2)_n=(\Omega^2_{n+1}-\Omega^2_n)$ between neighboring eigenvalues. (a) Symmetric prefractal system No. 1; (b) symmetric prefractal system No. 2; (c) quarter prefractal system No. 3; (d) quarter prefractal system No. 4.

increase of $C(\Omega^2)_{\text{No. 1}}$ is of the order of 10, a number comparable to the number of identical pores. For comparison we also calculated the correction term $C(\Omega^2)_{\text{No. 5}}=N(\Omega^2)_{\text{No. 5}}-N(\Omega^2)_{\text{No. 0}}$ for the 120 lower states of system No. 5 which has only four pores of width $L/4$. Indeed we find fluctuations at the same frequencies but with about half the amplitude.

For system No. 2, the width of the smallest pore is $L/16$. We therefore expect an oscillation at $\Omega^2=256$, but this value is beyond our calculated values. We think that the minor oscillations that we observe for this system are reminiscent of the $L/4$ pore of the first generation disturbed here by the second-order pattern.

Furthermore, there exist two steplike increases of the DOS around $\Omega^2\approx 7$ and $\Omega^2\approx 37$. One can understand these steplike increases by looking at the amplitude distributions of these eigenmodes: all modes with $\Omega^2\approx 7$ and all modes with $\Omega^2\approx 37$ look very similar and are localized at the boundary. We show one example for each frequency in Figs. 4(a) and 4(b), where the amplitudes are indicated by different gray levels. The black and white regions stand, respectively, for positive and negative amplitudes. The gray tones stand for nearly zero amplitude. For these states, the half wavelength should be of the order of the length of the path $\mathcal{L}$, connecting nearest black and white extrema. To illustrate this idea we have drawn in Figs. 4(a′) and 4(b′) paths which satisfy approximately $\Omega^2\approx 7$ and $\Omega^2\approx 37$. In Fig. 4(a′), $\mathcal{L}$ is about $3L/8$ and $[L/\mathcal{L}]^2$ is of order 8. The path $\mathcal{L}$ shown in Fig. 4(b′) corresponds to $[L/\mathcal{L}]^2\approx 35$.

The accumulation of states for these special values of Ω^2 reflects both the symmetry degeneracy and the fact that regions near the frontier may have similar shape and size even if not equivalent under a symmetry operation. For example, regions P_1 and P_2 in Figs. 4(a) and 4(b) may sustain quasidegenerated eigenmodes. This accumulation should therefore be a general feature of deterministic fractal structures, as discussed in Refs. [18, 22, 23], but should not exist in random fractals.

LEVEL SPACING DISTRIBUTION

Besides an accumulation of eigenstates at certain frequencies, we find occasionally very large distances between neighboring frequencies. This fact has to be considered in the framework of quantum chaos studies. The level distance statistics is an important tool to separate chaotic from regular systems [21]. In Fig. 5 we show the statistics of the level spacing $(\Delta\Omega^2)_n\equiv(\Omega^2_{n+1}-\Omega^2_n)$ in the form of histograms counting the number N of values $(\Delta\Omega^2)_n$ in a given interval.

In Figs. 5(a) and 5(b) we show the histograms for the symmetric systems No. 1 and No. 2. In these cases the values of $(\Delta\Omega^2)_n=0$ due to the degenerated states have been dropped. The spacing distribution of the symmetric systems resembles the Poisson distribution $N(\Delta\Omega^2)\propto\exp[-(\Delta\Omega^2)]$ generally expected for regular, nonchaotic systems. However, the C_4 symmetry of our prefractal systems disturbs the statistics as our data contain four series of eigenstates of different symmetry which overlap.

For this reason we also computed the eigenstates of systems No. 3 and No. 4. Their spacing distribution [Figs. 5(c) and 5(d)] shows a remarkably different behavior. First, the maximum of $N(\Delta\Omega^2)$ is shifted from zero to higher values while the probability of finding very small level differences between neighboring states is considerably diminished. Secondly, the probability of finding very large level spacings is smaller for the nonsymmetric systems. Consequently, $N(\Delta\Omega^2)$ is closer to the Gaussian orthogonal ensemble, which is typical for chaotic systems [21]. Note that eigenstates with very close frequencies are still present in the nonsymmetric systems due to the existence of nearly equivalent regions like P_1 and P_2 in Fig. 4. This is not the usual behavior of chaotic systems, which should show a ''level repulsion.'' For a random irregular system the quasidegeneracies associated with the similarity between P_1 and P_2 regions should disappear and the level repulsion should be more apparent.

Indeed our prefractal systems are pseudointegrable in the

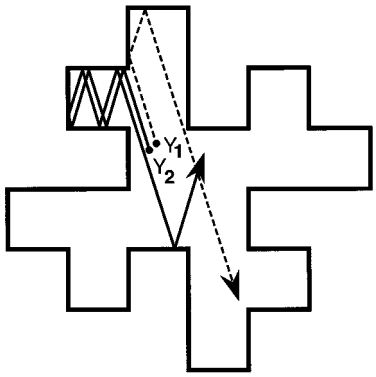

FIG. 6. Illustration of the beam splitting at a salient corner in a prefractal billiard. Depending on whether a particle arrives on the left- or on the right-hand side of the corner, it is reflected in two different directions.

sense of Richens and Berry [24,25]. The term ''pseudointegrable'' describes billiard problems in two-dimensional polygon enclosures whose angles are rational multiples of π and which have the additional property of ''beam splitting.'' This means that neighboring trajectories can split at salient corners as illustrated in Fig. 6. It was shown that for two-dimensional (2D) pseudointegrable systems, the trajectories in phase space are restricted to two-dimensional surfaces—as for integrable systems—but these surfaces do not have the shape of tori [24]. The behavior of pseudointegrable systems can be considered as intermediate between regular and chaotic. There is an apparent correspondence between the spacing distribution we found and the pseudointegrable character of our systems. By going from one prefractal generation to the next, the chaotic behavior should increase, as more and more salient corners appear.

WAVE FORMS AND LOCALIZATION

In this section we discuss the confinement of the vibrations. To characterize mathematically the localization or the confinement of each state we compute, following Thouless [26], the ''existence volume'' V_n of a given state Ψ_n by a sum on the lattice sites i,

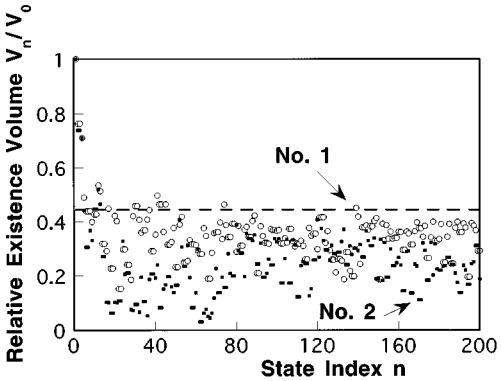

FIG. 7. Relative existence volume V_n/V_0 for the first 200 states of systems No. 1 and No. 2 computed from Eqs. (11) and (12). The value 4/9 for the square (No. 0) is indicated by the dashed line.

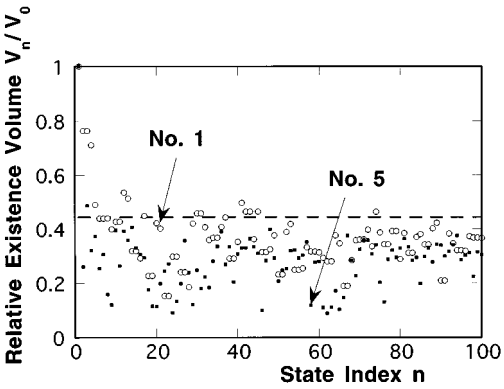

FIG. 8. Relative existence volume V_n/V_0 for the first 100 states of systems No. 1 and No. 5. The value 4/9 for square (No. 0) is indicated by the dashed line.

$$V_n=\left(\sum_i a^2|\Psi_{n,i}|^4\right)^{-1}, \tag{11}$$

where a is the lattice constant and Ψ_n is normalized by

$$\sum_i a^2|\Psi_{n,i}|^2=1. \tag{12}$$

The volume V_0 of a normalized constant function (like the trivial mode) is equal to the product of a^2 by the total number of particles. For a square with Z segments per side, $\Psi_{n,i}=a^{-1}(Z+1)^{-1}$ and $V_0=a^2(Z+1)^2=L^2$. If we find that V_n is significantly smaller than V_0 we say that the corresponding state of index n is ''localized.'' Figure 7 gives the values of the relative occupation volume V_n/V_0 of the first 200 lower states for the symmetric systems No. 1 and No. 2. Figure 8 gives the values for system No. 1 and for the nonsymmetric system No. 5. In both cases the results show that, apart from the very first states, the existence volume is only a fraction of the total surface of the resonator. In our systems the tendency to localization is increased by the irregularity of the frontier. Increasing the fractality has qualitatively the same effect on localization as lowering the symmetry. This important result confirms that deterministic fractality has the same qualitative effect as disorder.

For the symmetric system No. 1 the average $\langle V_n/V_0\rangle$ is found to be equal to 0.35. The corresponding value for the delocalized cosine functions of the square is $V_n/V_0=4/9=0.44$ as indicated by a dashed line in Figs. 7 and 8.

The highest degree of localization is found for system No. 2, for which the smallest value V_n/V_0 is equal to 0.031 for degenerated states $n=62$, 63. The average value of $\langle V_n/V_0\rangle$ over the 200 lower states is equal to 0.24. For the nonsymmetric system No. 5, the smallest value of V_n/V_0 is 0.088 for state index $n=62$ and the average $\langle V_n/V_0\rangle=0.28$.

We now discuss the spatial location of the modes. Whereas Dirichlet fractinos decay very rapidly towards the boundary [12] Neumann fractinos have the opposite tendency: as the boundary is free to vibrate, eigenmodes can have a maximum amplitude at this location. The existence of these states can be understood from the observation of region P_1 of Figs. 4(a) and 4(b). For such states, the diffusion from regions with positive concentration towards regions of nega-

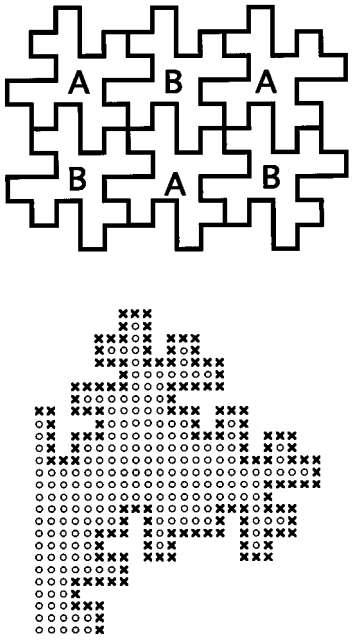

FIG. 9. Top: Scheme of a dense material with irregular or fractal interfaces. Bottom: Partial scheme of the atomic structure of a crystallite with geometry No. 2 with three atoms on the smaller cut-off. For a Dirichlet crystallite the perimeter atoms, here represented by bold ×, are kept fixed. For a Neumann crystallite the perimeter atoms are free to move.

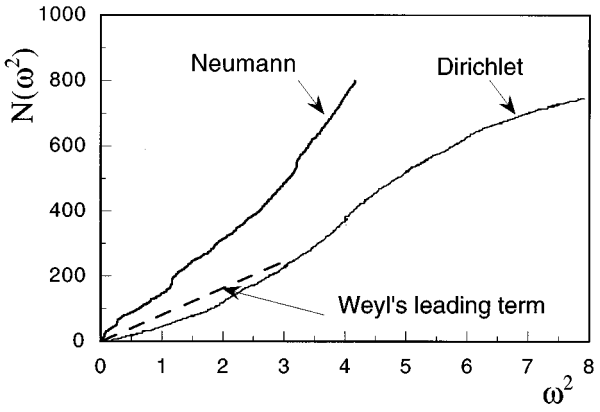

FIG. 10. Neumann and Dirichlet integrated DOS (with the *same* spring constant) for the small crystallite partially depicted by Fig. 9, bottom. The horizontal coordinate is given in computer units as discussed in the Appendix. The dashed line represents Weyl's leading term.

tive concentration occurs between neighboring pores. Then, a small particle concentration in the interior of the system is compatible with a large concentration near the boundary. Most of the localized states are located in this manner near the frontier. In the vibrational picture, one can think that waves being excited in the small pores are submitted to multiple diffraction which may cause partially destructive interferences in the central region of the system. This is a weak localization effect which does not occur for all states. Note that if no rotation degeneracy existed, the localization volume for these states would be typically four times smaller than the values found in system No. 2.

When the fractal character of the frontier increases we find more and more surface modes. This is an important property of the Neumann fractinos. Qualitatively, the more irregular and winding the boundary, the more localized many of the Neumann fractinos. We expect a similar behavior for 3D irregular systems. As these modes represent transverse acoustical phonons, the increased localization may show up as a decrease of the heat conduction of irregular crystallites at low or average temperature ($T<50$ K). Due to localization near irregular boundaries, Neumann fractinos should not propagate as ordinary phonons and the heat conductivity of a small crystallite should depend on its geometrical irregularity.

DISCUSSION OF SMALL IRREGULAR CRYSTALLITE VIBRATIONS

The modification of the DOS due to the resonator shape, also observed for Dirichlet fractinos [12], could help in understanding the vibrational properties of strongly inhomogeneous solids like demixed glasses [27]. In such binary solids, there exist separated *A* and *B* regions, principally made up of *A* atoms or *B* atoms. Although the mass distribution is nonfractal, the internal interfaces between the *A* and *B* regions may be irregular and even possibly fractal [28,29]. The discussion that we present below has been suggested by the observed anomalous vibrations in the amorphous superionic glass $(AgI)_x(Ag_2O,B_2O_3)_{1-x}$ [30,31]. This glass is a collection of irregular domains principally composed of AgI and Ag_2O,B_2O_3 and could present irregular interfaces between domains. The extremely high ionic conductivity shows that the Ag^+ ions (at least in the AgI regions) are weakly coupled to the cage. One has then a strong contrast between the coupling constants of the different atoms.

A schematic picture of such a hypothetical 2D solid is shown in Fig. 9, top. As represented, the figure shows a crystalline arrangement but we keep in mind a disordered structure. We have computed the vibrations of a 2D structure in which Dirichlet and Neumann fractinos can both exist. This is the case if the local vibrational properties of *A* and *B*

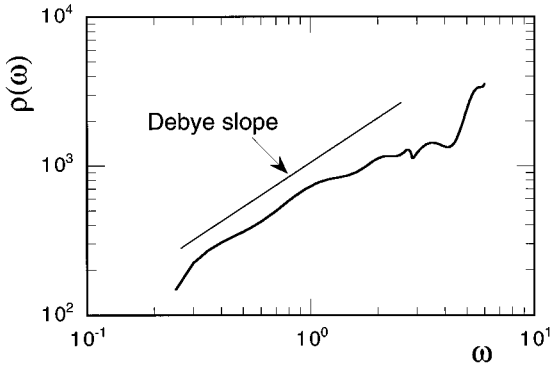

FIG. 11. Differential density of states of a collection of Dirichlet crystallites (with *soft* springs) and Neumann crystallites (with *stiff* springs). The dashed line indicates the usual Debye slope in $d=2$. Note the break around $\omega=3$. The horizontal coordinate is given in computer units as discussed in the Appendix.

TABLE I. The lowest eigenvalues of several vibrating systems under Neumann boundary conditions (in reduced units). The first column (a) gives the index (or integrated DOS) of the state. Column (b) gives the exact eigenvalues for the continuous square. Column (c) gives the exact result from Eq. (6) for the discretized square with $Z=64$. Columns (d), (e), and (f) give, respectively, the numerical eigenvalues for system No. 0 with $Z=64$ and systems No. 1 and No. 2 with $Z=128$. Tables giving the ensemble of our results are available upon request.

(a) Index	(b) $(\mu^2+\mu'^2)$	(c) Eq. (9)	(d) No. 0	(e) No. 1	(f) No. 2
1	1.0	0.999 805 348	0.998 053 50	0.395 335 034	0.309 143 059
2	1.0	0.999 805 348	0.998 053 50	0.395 335 034	0.309 143 059
3	2.0	1.999 610 70	1.999 610 70	0.485 888 934	0.363 068 740
4	4.0	3.996 886 30	3.996 886 31	2.061 221 08	1.501 785 36
5	4.0	3.996 886 30	3.996 886 31	2.454 292 45	1.727 122 82
6	5.0	4.996 691 65	4.996 691 65	2.454 292 45	1.727 122 82
7	5.0	4.996 691 65	4.996 691 65	2.471 316 62	1.736 189 83
8	8.0	7.993 772 60	7.993 772 59	2.699 429 97	1.928 338 50
9	9.0	8.984 243 04	8.984 243 04	5.389 272 47	3.979 217 83
10	9.0	8.984 243 04	8.984 243 04	5.389 272 47	3.979 217 83
11	10.0	9.984 048 39	9.984 048 37	7.080 594 34	4.493 104 96
12	10.0	9.984 048 39	9.984 048 37	9.086 646 92	5.150 893 91
13	13.0	12.981 129 3	12.981 129 4	10.710 063 5	6.394 524 87
14	13.0	12.981 129 3	12.981 129 4	10.710 063 5	6.394 524 87
15	16.0	15.950 227 4	15.950 227 3	12.629 351 8	6.827 878 37
16	16.0	15.950 227 4	15.950 227 3	15.713 986 0	6.829 816 12
17	17.0	16.950 032 7	16.950 032 7	15.913 258 0	6.829 816 12
18	17.0	16.950 032 7	16.950 032 7	15.913 258 0	6.833 741 60
19	18.0	17.968 486 1	17.968 486 1	15.694 466 1	6.839 132 75
20	20.0	19.947 113 7	19.947 113 7	16.159 403 6	6.839 132 75

are strongly contrasted, for example, if the A-A and A-B springs are very soft and the B-B springs very stiff.

First, we compute the Dirichlet and Neumann fractinos DOS (with the *same* spring constant k) for a single 2D crystallite with geometry No. 2 and having only three atoms on the smallest segment. A part of this structure is depicted in Fig. 9, bottom. Note that we are computing here a naturally discretized atomic structure. The results are shown in Fig. 10 together with the Weyl leading term which represents the classical Debye behavior and neglects both crystalline dispersion and irregularity. One observes that the Neumann DOS is always larger than the Debye DOS while the Dirichlet DOS is smaller at low frequency. These data cannot be simply extended to the case of a real 3D material because of the existence of various modes and polarization of vibrations in solids.

Instead, from the data of Fig. 10 we compute the differential DOS of a collection of one Dirichlet 2D crystallite with spring constant k (supposedly representing the Ag^+ ions in AgI) and ten Neumann 2D crystallites with spring constant $9k$ (supposedly representing the rest of the glass). The result is shown in Fig. 11. One observes a break in the DOS curve. At low frequency the average slope is slightly smaller than the Debye slope (equal to 1 in $d=2$) while above $\omega\approx 3$ the DOS presents a more rapid dependence. This behavior, although 2D, is similar to the behavior of the DOS of $(AgI)_x(Ag_2O,B_2O_3)_{1-x}$ determined by inelastic neutron scattering [30,31]. This material presents an anomalous DOS: below 1 meV it exhibits an under-Debye behavior (ω^α with $\alpha<2$). For higher frequencies (above 1 meV) the observed α is larger than 2 and the DOS increases faster than in the ordinary Debye 3D case. At still higher frequencies the DOS is compatible with the fracton density of states.

Another possible consequence of the existence of Dirichlet and Neumann fractinos could be to lower the heat conduction. Because Dirichlet fractinos have a tendency to be localized in the internal region of the resonator [12] and Neumann fractinos are localized near the boundary, their coupling should be small. Hence one predicts that the existence of such internal irregularity should contribute to lower the heat conduction.

CONCLUSIONS AND OUTLOOK

We have studied vibrational modes of 2D irregular structures obeying the Neumann boundary condition. There are two main effects due to the boundary irregularity.

First there exists an increase in the density of states in agreement with Weyl's conjecture but presenting strong oscillations in deterministic prefractal geometries. Second and more surprising, we have found many modes which are confined near the fractal boundary. This localization effect increases from one fractal generation to the next, even for deterministic prefractals. This shows that fractality has the same qualitative effect as disorder.

This localization should exist in irregular acoustical cavities where the acoustic pressure obeys the Neumann condition on rigid boundaries. A straightforward example is an

TABLE II. Comparison of the eigenvalues computed using predetermined precision and predetermined number of steps. The calculations are performed on the prefractal system No. 2 with $Z=64$. In the first column the iteration process has been continued until a predetermined precision $\Delta=0.5\times10^{-6}$ has been reached. In the second column the iteration process is automatically stopped after 5 020 000 iterations. The subcolumns indicate the number of iterations and the respective eigenvalue. It can be seen that the few states with restricted number of iterations show comparatively large errors but that this does not modify higher eigenvalues.

	(a)		(b)	
State	Iterations	Ω^2	Iterations	Ω^2
60	780 000	34.069 901 6	780 000	34.069 901 6
61	65 760 000	34.816 274 5	5 020 000	34.817 434 6
62	151 760 000	34.817 987 3	5 020 000	34.817 857 8
63	151 760 000	34.817 987 3	5 020 000	34.817 951 2
64	28 820 000	34.818 083 7	5 020 000	34.818 319 9
65	480 000	34.818 719 9	5 020 000	34.818 452 0
66	260 000	34.819 177 1	5 020 000	34.818 715 4
67	260 000	34.819 177 1	5 020 000	34.818 723 3
68	320 000	34.823 693 0	340 000	34.823 646 5
69	260 000	35.918 228 3	380 000	35.918 228 3
70	220 000	36.819 475 0	1 840 000	36.819 475 0
71	340 000	37.411 440 0	340 000	37.411 440 0
.	.	.	.	.
.	.	.	.	.
.	.	.	.	.
78	100 000	42.465 272 0	100 000	42.465 272 0
79	100 000	43.286 617 3	100 000	43.286 617 3
.	.	.	.	.
.	.	.	.	.
.	.	.	.	.
105	1 150 000	79.034 979 3	1 310 000	79.034 979 3
106	220 000	79.339 022 4	220 000	79.339 022 4
107	220 000	79.339 022 4	220 000	79.339 022 4

acoustic waveguide with prefractal cross section for which many of the so-called higher modes would be localized in different regions.

Using our simple 2D results, we have discussed the possible influence of the interface irregularities on the vibrational properties of demixed binary solids. To the extent that our conclusions still hold in $d=3$, this gives a first hint to understand the anomalous vibrational properties of superionic glasses like $(AgI)_x(Ag_2O,B_2O_3)_{1-x}$.

The localization effects should also play a role in the heat conductivity of small irregular crystallites and contribute to lowering the heat conduction of binary glasses. The same localization effects could play a role in the electron-phonon coupling in irregular crystallites.

ACKNOWLEDGMENTS

We gratefully acknowledge valuable discussions with M. L. Lapidus. One of us (S.R.) has benefited from the E.E.C. program ''Human Capital and Mobility.'' The computation was performed at the ''Institut du Développement et des Ressources en Informatique Scientifique'' (IDRIS) in Orsay, France.

APPENDIX: COMMENTS ON THE NUMERICAL METHOD

We compute the time evolution of the numerical solution of Eq. (3) on a discretized grid until we obtain everywhere a single exponential decay. Our precision criterion is the comparison of the time evolution of the concentration Ψ_i on the different grid sites i, which we compute until it is the same everywhere within a predetermined relative error Δ, generally chosen as $\Delta=0.5\times10^{-6}$ [12].

The computer time step (the relative increase in time between two consecutive readjustments of the values of Ψ at the lattice sites) was chosen equal to $\tau_s/10$ where τ_s is the inverse of the jump probability per unit time W. The diffusion coefficient in $d=2$ is given by $D=a^2/4\tau_s$ and for a given state Ψ_n the computer time constant τ_n is given in units of τ_s. From the relation (4) the corresponding eigenvalue is $\omega_n^2=4(\tau_s/\tau_n)(c/a)^2$ or $\omega_n^2=4/\tau_n$ in computer units ($c=1$; $a=1$; $\tau_s=1$). Note that both ω_n^2 and τ_n depend on the number $Z=L/a$ of segments on the side of the initial square. The value of the fundamental time constant $\tau_{1,0}=L^2/\pi^2D$ is given by $(2Z/\pi)^2$ in computer units.

Discretization in space introduces a difference with continuous systems. For the square, exact solutions exist for both the continuous and the discretized cases and this difference is known exactly.

Numerical errors are due to convergence limitations. For the square, these errors can be monitored by comparing numerical values with the exact values from Eq. (7). Table I gives the 20 lower eigenvalues for the different systems. Column (b) shows the values for the continuous square system, column (c) the exact solutions [Eq. (7)] for the discretized square with $Z=64$, and column (d) shows the numerical values for the same discretized square. The first 20 values for systems No. 1 and No. 2 are given in columns (e) and (f). The difference between (b) and (c) is due to discretization. The comparison between exact and numerical values—columns (c) and (d)—gives a measure of our precision. The largest relative deviation is of order 10^{-9}. Even for higher eigenvalues the precision is very good in the case of the square. For example, for state number 206 ($\mu=\mu'=11$), the exact value from Eq. (6) is $\Omega^2(11,11)=236.353\,204\,932$ and its numerical approximation is 236.353 204 964. The relative error of order 10^{-10} indicates the reliability of our method.

For our systems, we observed that quasidegeneracy induces a considerable increase in the computation time. If there exist two states Ψ_a and Ψ_b, with close time constants τ_a and τ_b and if we start with $(\Psi_a+\Psi_b)$ at time $t=0$, the function will be at time t equal to

$$\Psi_a\exp(-t/\tau_a)+\Psi_b\exp(-t/\tau_b)$$

$$=(\exp[-t/\tau_a])\{\Psi_a+\Psi_b\exp[-t(\tau_a-\tau_b)/\tau_a\tau_b]\}.$$

Therefore many iterations are needed before $\exp[-t(\tau_a-\tau_b)/\tau_a\tau_b]$ is small enough to reach a single exponential decay. Table II gives the number of steps needed to reach the required precision for system No. 2 with $Z=64$.

States 61–68 are degenerate or quasidegenerate and require 100–1000 times more steps than normal states. (True degeneracy due to the system symmetry is not a difficulty if one starts with appropriate symmetrized functions [12].)

To shorten the computation time we have restricted the procedure to a predetermined limited number of steps instead of predetermined precision. Doing that, we accept a lower precision for the quasidegenerated states, hoping that this will not modify higher states and eigenvalues as we discuss below. The results are shown in Table II(b), where the number of steps was limited to 5 020 000. Comparison of columns (a) and (b) shows that, beyond state 69, there is very little perturbation. We controlled this for about 200 states with a precision of nine digits. These results indicate the robust character of our numerical procedure. We found a number of these quasidegenerated states for systems No. 2 and No. 5. Using a predetermined limited number of steps equal to 5 020 000 we computed 214 eigenstates within about 10 h on a Cray C98 vector processor.

In our method, the numerical eigenvalues are a *result* of the computation but do not enter into the numerical process itself. To compute Ψ_{n+1} and Ω_{n+1}^2 we do not need the n previous eigenvalues or the n previous eigenfunctions but only an orthogonal basis in the subspace generated by the true eigenfunctions. If we stop the computation before convergence we obtain an orthogonal basis of functions $|X_\nu\rangle = |c_{\nu,1}\Psi_1 + c_{\nu,2}\Psi_2 + \cdots + c_{\nu,n-1}\Psi_{n-1}\rangle$ which are not eigenstates but linear-independent combinations of these eigenstates. To compute the nth eigenstate $|\Psi_n\rangle$ we start with an arbitrary function $|z_n\rangle$ that we orthogonalize to all lower states $|X_\nu\rangle$. If $|z_n\rangle$ is orthogonal to all $|X_\nu\rangle$, we have

$$c_{1,1}\langle z_n|\Psi_1\rangle + c_{1,2}\langle z_n|\Psi_2\rangle + \cdots + c_{1,n-1}\langle z_n|\Psi_{n-1}\rangle = 0,$$

$$\cdots\cdots\cdots\cdots\cdots$$

$$c_{n-1,1}\langle z_n|\Psi_1\rangle + c_{n-1,2}\langle z_n|\Psi_2\rangle + \cdots + c_{n-1,n-1}\langle z_n|\Psi_{n-1}\rangle = 0.$$

This set of linear equations with unknowns $\langle z_n|\Psi_\nu\rangle$ has a nonzero determinant because of the linear independence of the vectors $|X_\nu\rangle$. Hence the only solution is $\langle z_n|\Psi_\nu\rangle = 0$ for all ν. Note that orthogonalizing $z_n(x,y,t=0)$ to the normalized constant state Ψ_0 is equivalent to subtracting its space average $\langle\Psi_0\rangle$ from $z_n(x,y,t=0)$. For this reason we chose the first initial distribution $z_0(x,y,t=0)$ not as a constant.

In conclusion, *as long as we are working in the same subspace*, the use of an eigenstate basis is not necessary. Restricting the computation time induces errors for the eigenvalues in this subspace, but does not induce errors for higher eigenvalues.

[1] B. Mandelbrot, *The Fractal Geometry of Nature* (Freeman, San Francisco, 1982).

[2] B. Sapoval, *Fractals* (Aditech, Paris, 1990).

[3] B. Sapoval, Phys. Rev. Lett. **73**, 1570 (1994).

[4] M. V. Berry, in *Structural Stability in Physics*, edited by W. Guttinger and H. Elkeimer (Springer-Verlag, Berlin, 1979), pp. 51–53.

[5] M. L. Lapidus, Trans. Am. Math. Soc. **323**, 465 (1991), and references therein.

[6] J. Brossard and R. Carmona, Commun. Math. Phys. **104**, 103 (1986).

[7] M. L. Lapidus and C. Pomerance, Proc. London Math. Soc. **3**, 41 (1993).

[8] H. P. Baltes and E. R. Hilf, *Spectra of Finite Systems* (BI Wissenschaftsverlag, Vienna, 1976).

[9] S. Alexander and R. Orbach, J. Phys. (Paris) Lett. **43**, L625 (1982).

[10] R. Rammal and G. Toulouse, J. Phys. (Paris) Lett. **44**, L13 (1983).

[11] T. Nakayama, K. Yakubo, and R. L. Orbach, Rev. Mod. Phys. **66**, 381 (1994).

[12] B. Sapoval and Th. Gobron, Phys. Rev. E **47**, 3013 (1993).

[13] B. Sapoval, Th. Gobron, and A. Margolina, Phys. Rev. Lett. **67**, 2974 (1991).

[14] B. Sapoval and S. Russ, in *Microcrystalline and Nanocrystalline Semiconductors*, edited by L. Brus *et al.*, MRS Symposia Proceedings No. 358 (Materials Research Society, Pittsburgh, 1995), pp. 37–42.

[15] B. Sapoval and S. Russ, in *Disordered Materials and Interfaces*, edited by H. E. Stanley *et al.*, MRS Symposia Proceedings No. 407 (Materials Research Society, Pittsburgh, 1996), pp. 253–257; and B. Sapoval, S. Russ, and J.-N. Chazalviel, J. Phys. C **8**, 6235 (1996).

[16] P. M. Morse and K. Uno Ingard, *Theoretical Acoustics* (Princeton University Press, Princeton, NJ, 1968).

[17] M. Born and Th. von Karman, Phys. Z. **13**, 297 (1912).

[18] J. Hobiki, K. Yakubo, and T. Nakayama, Phys. Rev. E **54**, 1997 (1996).

[19] M. F. Fisher, J. Comb. Theory **1**, 105 (1966).

[20] J. Hobiki, K. Yakubo, and T. Nakayama, Phys. Rev. E **52**, R1310 (1995).

[21] M. C. Gutzwiller, J. Math. Phys. **12**, 343 (1971).

[22] M. Levitin and D. Vassiliev, Proc. London Math. Soc. **72**, 178 (1996).

[23] J. Fleckinger, M. Levitin, and D. Vassiliev, Proc. London Math. Soc. **71**, 372 (1995).

[24] P. J. Richens and M. V. Berry, Physica D **2**, 495 (1981).

[25] A. Kudrolli, S. Shridar, A. Pandey, and R. Ramaswamy, Phys. Rev. E **49**, R11 (1994).

[26] D. J. Thouless, Phys. Rep. **13**, 93 (1974).

[27] *Phase Separation in Glass*, edited by O. V. Mazurin and E. A. Porai-Koshits (North-Holland, Amsterdam, 1984).

[28] B. Sapoval, M. Rosso, and J.-F. Gouyet, in *The Fractal Approach to Heterogeneous Chemistry*, edited by D. Avnir (Wiley, New York, 1989), p. 227, and references therein.

[29] B. Sapoval, Physica A **191**, 321 (1992).

[30] A. Fontana, F. Rocca, M. P. Fontana, B. Rosi, and A. J. Dianoux, Phys. Rev. B **41**, 3778 (1990).

[31] M. P. Fontana, B. Rosi, A. Fontana, and F. Rocca, Philos. Mag. B **65**, 143 (1992).